

# Sensing Finger Input Using An RFID Transmission Line

Ju Wang<sup>1</sup>, Jianyan Li<sup>1</sup>, Mohammad Hossein Mazaheri<sup>1</sup>,  
Keiko Katsuragawa<sup>1,2</sup>, Daniel Vogel<sup>1</sup>, and Omid Abari<sup>3</sup>

<sup>1</sup>University of Waterloo, <sup>2</sup>National Research Council Canada, <sup>3</sup>University of California, Los Angeles  
{ju.wang, Mohammad.Mazaheri, kkatsuragawa, dvogel}@uwaterloo.ca  
jianyan.li@edu.uwaterloo.ca,omid@cs.ucla.edu

## ABSTRACT

We introduce a passive Radio Frequency Identification (RFID) based system to detect finger gesture input for Human-Computer Interaction applications. The device is simple, inexpensive and does not require calibration to accommodate changes in the device location or the Radio Frequency (RF) environment. This is achieved by connecting the chips of two RFID tags together using a strip transmission line. The key observation is that touching different positions along the transmission line changes the impedance matching between each chip and its antenna, changing Received Signal Strength (RSS) values for each tag. When a finger slides in different directions between key positions along the transmission line, there are relative RSS patterns and trends that are robust to changes in the device location and the RF environment. We implemented and evaluated an detection algorithm and system using a commercial RFID reader and two commercial RFID chips. Results show that precision and recall are greater than 95% and 94% when detecting 10 finger gesture inputs across 48 different device locations.

## CCS CONCEPTS

• **Computer systems organization** → *Sensor networks*.

## KEYWORDS

Finger Input, Gesture, RFID, Transmission Line

### ACM Reference Format:

Ju Wang<sup>1</sup>, Jianyan Li<sup>1</sup>, Mohammad Hossein Mazaheri<sup>1</sup>, and Keiko Katsuragawa<sup>1,2</sup>, Daniel Vogel<sup>1</sup>, and Omid Abari<sup>3</sup>. 2020. Sensing Finger Input Using An RFID Transmission Line. In *The 18th ACM Conference on Embedded Networked Sensor Systems (SenSys '20)*, November 16–19, 2020, Virtual Event, Japan. ACM, New York, NY, USA, 13 pages. <https://doi.org/10.1145/3384419.3430712>

## 1 INTRODUCTION

With an increasing number of smart devices, such as smart televisions, thermostats, and light bulbs, there is significant interest in finding new user input methods to control them. Using a smartphone or voice assistant is not always practical, convenient, or

This article was authored by employees of the Government of Canada. As such, the Canadian government retains all interest in the copyright to this work and grants to ACM a nonexclusive, royalty-free right to publish or reproduce this article, or to allow others to do so, provided that clear attribution is given both to the authors and the Canadian government agency employing them. Permission to make digital or hard copies for personal or classroom use is granted. Copies must bear this notice and the full citation on the first page. Copyrights for components of this work owned by others than the Canadian Government must be honored. To copy otherwise, distribute, republish, or post, requires prior specific permission and/or a fee. Request permissions from [permissions@acm.org](mailto:permissions@acm.org).

*SenSys '20, November 16–19, 2020, Virtual Event, Japan*

© 2020 Crown in Right of Canada.

ACM ISBN 978-1-4503-7590-0/20/11...\$15.00

<https://doi.org/10.1145/3384419.3430712>

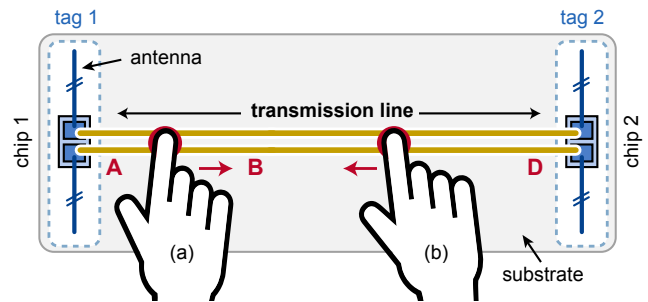


**Figure 1: The touch input sensing device is created by connecting the chips of two RFID tags together with copper strips to form a transmission line. When a finger is sliding in different directions between key known positions, e.g. (a) A-to-B or (b) D-to-B, relative RSS patterns for each chip can be used for gesture detection independent of changes to device location or RF environment.**

comfortable for issuing commands in this setting. Smartphone apps can be hard to configure, they are not easily shared among roommates or co-workers, and they take time to open and navigate. Speaking to a voice assistant can feel socially uncomfortable, and relatively simple operations, like setting the brightness of a specific light, are surprisingly verbose. For these and other reasons, other general purpose user input methods have been proposed to sense finger input gestures, primarily based on computer vision [15, 21], mmWave [18], Wi-Fi [7], and RFID [16] technologies. Of these approaches, a system based on RFID is particularly attractive since it is wireless, battery-free, lightweight, and very low cost [14, 17, 20]. RFID tags can be embedded into common objects, like cups and doorknobs, to enable sensing and interaction.

However, a general purpose RFID-based finger input sensing device for these kinds of applications has two challenges. The device should detect multiple gesture inputs to be useful as a kind of remote control for smart devices, and it should be robust to changes in device position and the surrounding RF environment (e.g. people moving nearby) since many smart device applications are used in a more mobile setting. Accomplishing both of these without adding more and more RFID tags, or requiring frequent calibration and training, has not been achieved before.

For example, PaperID [16] uses an RFID tag as a binary sensor to detect when a finger is touching, so it requires many tags to detect multiple finger inputs. RIO [20] can detect multiple inputs on a single tag using the phase of the RFID signal, but this is not robust to changes in the tag location or RF environment without frequent device re-calibration and retraining. These limitations

are because *absolute* phase or RSS is used for detection. Previous systems rely on how touching different positions along an RFID tag antenna changes the impedance matching between the RFID chip and its antenna, which changes the RSS or phase of the tag response signal [16, 17, 20]. The problem is that changes in the tag location or RF environment also significantly alter the RSS and phase [24]. This is why past systems are not robust to such changes, and they require re-calibration and re-training.

Our approach attaches two RFID chips to a substrate and connects them with two thin strips of copper to form a *transmission line* (see Fig. 1 and demo video [28]). This enables our system to exploit the *trend* of RSS and *relative* RSS values in each of the connected RFID chips. When a finger slides between different positions along the transmission line, the finger movement changes the impedance matching between each RFID chip and its antenna continuously, and thus the momentary trend of RSS will increase or decrease continuously, no matter where the tag is located and the RF environment is changed or not. By defining a set of 10 short finger sliding gestures<sup>1</sup> that connect (or cross) key positions along the transmission line, we show that a novel algorithm can detect these gestures using features based on relative changes and trends in RSS. This means the detection method is independent of tag location and RF environment, so the device does not require re-calibration or re-training. This enables user input for many smart device applications. For example, our device can be used like a remote control or integrated into household items such as a pillow, book, or chair, enabling the remote adjustment of smart device properties like light intensity, room temperature, or TV volume, or in settings like a lecture hall for an audience response system.

We provide the underlying theory and initial data gathering experiments to explain how and why our approach works. We also describe the prototype device we built with two commodity RFID chips [6] and available materials like cardboard and copper tape. Using a system with Impinj RFID readers [10], we evaluate our prototype in two indoor settings: a laboratory area covered by one reader antenna and a large classroom covered by four reader antennas. Combined results spanning both environments show precision and recall are greater than 95% and 94% when detecting 10 finger gesture inputs across 48 different device locations.

Our main contributions are:

- An RFID-based finger input sensing system which eliminates the need for calibration and training using a transmission line.
- A set of finger input gestures with an associated detection algorithm designed to be reliably differentiate gestures.
- The implementation and evaluation of a prototype system shown to be robust to variations of device locations and RF environment.

## 2 RELATED WORK

RFID tags have been used to sense user input before, but existing methods have been limited by the input diversity or accuracy of the input detection or the method is not robust when there are changes in tag locations or the RF environment.

One set of techniques enable user input by tracking coarse movements of one or more tags attached to a hand or a finger. For example, Bainbridge *et al.* [2] use WISP RFID tags and 3-axis accelerometers attached to fingers for gesture recognition. However, the method also requires a powered RFID reader and antenna to be mounted on the arm and hand, limiting real-world applications. RF-IDraw [29] tracks the path of an RFID tag attached to the user's finger with 9.7 cm precision, and D-Watch [30] tracks a fist location with 5.8 cm precision using RFID tags placed in the surrounding environment. Given the very coarse level of tracking, neither method is well suited for the more fine-grained finger input.

IDSense [17] focuses on detecting a small set of discrete actions for input related to objects. The method attaches RFID tags to objects and uses multiple signal features (i.e., phase, RSS and reading rate) to detect four tag states with 95.7% accuracy: tag is moving, tag is covered by a hand, tag has been swiped by a finger, or none of the above. However, detection only works if the objects do not move after a calibration, which limits its applications.

Other papers have significantly expanded the touch input space beyond the single swipe gesture demonstrated by IDSense. For example, RIO [20] detects a finger touch and a swipe on RFID tags by tracking changes in phase values. Due to the fine-grained phase information, RIO can even locate finger touch positions with a 3mm accuracy in a controlled environment and a fixed tag location. However, phase values can vary as large as  $\pi$  rad with minor changes in the tag's location (e.g. 10 cm) [24]. Without re-calibration after the tag is moved, the input detection becomes unreliable, making it unsuitable for many real-world deployments.

PaperID [16] uses a simpler approach where a half-antenna design together with an RFID chip acts like a binary sensor capable of detecting when a finger is touching. Specifically, when their customized RFID tag is touched, the finger acts as another half-antenna, allowing the tag to harvest enough power for operation so that the RFID reader can hear the touched tag. The approach is robust to tag location changes. To increase input diversity, however, multiple tags must be used in a large array. The difficulty is that adjacent tags must be more than a half-wavelength apart to avoid a coupling effect [22, 23]. With the 915 MHz RFID signal, this translates to spacing at least 16.4 cm, which would create very large devices to support even a few different inputs. Second, for many handheld interactions, the size of input devices should be small. Tip-Tap [14] uses the connection and disconnection among multiple RFID chips for finger inputs. But the system requires 6 RFID chips to enable 9 finger inputs.

Compared to previous work, our system has two advantages. First, it requires only two RFID tags to detect 10 finger input gestures. Second, our method enables robust input detection even when tag location changes.

## 3 PASSIVE RFID BACKGROUND

A passive RFID system consists of a reader and one or more tags (Fig. 2). Each tag has an RFID chip, and a dipole antenna commonly composed of two identical conductive elements, such as metal wires [3]. 'Passive' means the tag has no battery. To power and activate the chip, the tag harvests energy from a reader transmitting high power signals. Once activated, the tag communicates

<sup>1</sup>Adding even one more chip in a triangle configuration could expand the input space to 30 gestures, we discuss this and other extensions in Section 8.

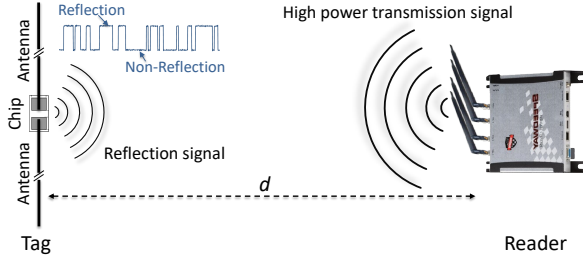


Figure 2: Illustration of a passive RFID system.

with the reader by reflecting or not reflecting the reader's signal. For example, a reflection represents a '1' bit and a not reflecting means a '0' bit.

### 3.1 RSS And Antenna Impedance

When an RFID reader receives a tag's reflection signal, the reader not only retrieves the tag's ID information, but also estimates RF characteristics like phase and RSS [24, 25]. The RSS is the power of a tag's backscatter signal received by an RFID reader, which can be expressed in dBm as [9]:

$$RSS = 10 \log \left| \frac{P_t G_t^2 \lambda^2 \sigma}{(4\pi)^3 d^4} \cdot \eta \right|, \quad (1)$$

where,  $P_t$  is the reader's transmission power,  $G_t$  is the gain of a reader's antenna,  $\lambda$  is the wavelength of RFID signal,  $\sigma$  is the radar cross section of the tag,  $d$  is the distance between the reader's antenna and the tag, and  $\eta$  is the impedance matching efficiency between a tag's chip and its antenna.

For the best impedance matching when  $\eta = 1$ , all electromagnetic waves absorbed by the tag's antenna are transferred to the chip, and the tag's RSS value reaches the maximum. In practice, the RSS value is less than the theoretical maximum due to various factors in the tag design. The matching efficiency  $\eta$  is related to the reflection coefficient  $\Gamma$  as follows:

$$\eta = 1 - |\Gamma|, \quad (2)$$

where  $|\Gamma| \leq 1$ . The reflection coefficient  $\Gamma$  is related to the impedance of the tag's antenna and the antenna's load. For an unmodified or conventional tag, this load is the impedance of an RFID chip. Fig. 3 shows an equivalent circuit of an RFID tag, where  $Z_a$  and  $Z_c$  are impedance of the antenna and the chip. Then, the reflection coefficient  $\Gamma$  can be expressed as [32]:

$$\Gamma = \frac{Z_c - Z_a}{Z_c + Z_a}. \quad (3)$$

When  $Z_c = Z_a$ , then  $\Gamma = 0$ , implying no reflected signal, so maximum power is delivered to the chip. By Eqn. (2), the best impedance matching is achieved since  $\eta = 1$ , and the RSS reaches the maximum value by Eqn. (1).

### 3.2 Input Impedance of A Transmission Line

A transmission line connects a pair of conductors to guide an electromagnetic wave from one end to the other, typically with minimum propagation loss into space and substrate. At high radio frequencies, the behaviour of signals in a transmission line is very different from that of ordinary wires carrying low-frequency signals. This is especially true when the physical dimension of a circuit is comparable

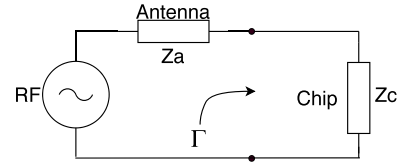


Figure 3: An equivalent circuit of an RFID tag.

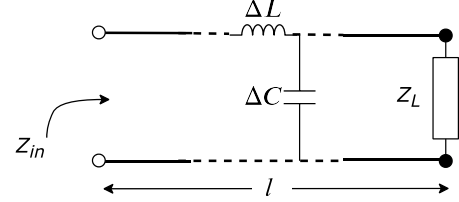


Figure 4: A lossless transmission line, length  $l$ , terminated with a load  $Z_L$ .  $\Delta L$  and  $\Delta C$  are the parasitic capacitance and inductance per unit distance.

to the wavelength of the radio signal. This is because passive parasitics, like inductance, capacitance, and resistance, are distributed along the length of the transmission line. Thus, the impedance of a transmission line become non-negligible for high frequency signals.

The input impedance of a transmission line is calculated as follows. Consider a lossless transmission line with length  $l$ , terminated with a load  $Z_L$ , as shown in Fig. 4. Due to capacitance and inductance per unit distance ( $\Delta L$  and  $\Delta C$ ), the input impedance  $Z_{in}$  is not equal to the load  $Z_L$ . Instead, the input impedance  $Z_{in}$  of a transmission line is [4]:

$$Z_{in} = Z_0 \cdot \frac{Z_L + jZ_0 \tan(\beta l)}{Z_0 + jZ_L \tan(\beta l)}, \quad (4)$$

where,  $Z_0$  is the characteristic impedance, which is a constant for a given transmission line, and  $\beta = \frac{2\pi}{\lambda}$ , where  $\lambda$  is the signal wavelength.

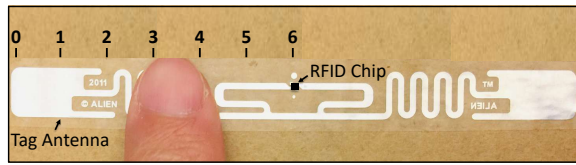
We return to these equations in Section 4.3 to explain why RSS changes in a predictable way when a finger touches on the transmission line between two tags.

## 4 TRANSMISSION LINE AS SENSORS

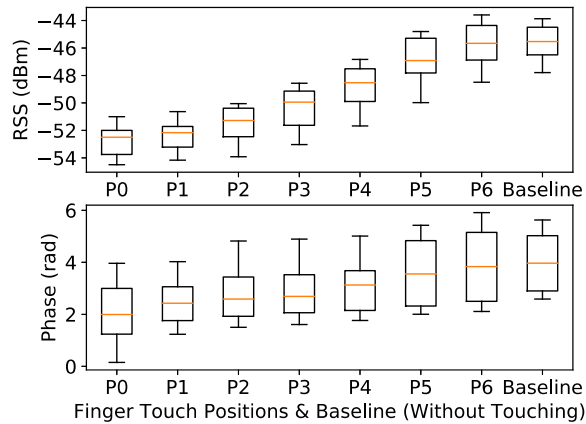
This section explains how an RFID transmission line can be used as a finger input sensor. We first motivate the need for our approach by giving inherent challenges if one use only an RFID tag as a sensor. Then, we provide the details of our prototype RFID transmission line device and show experimental results of RSS patterns when a finger touches different positions along the transmission line. Finally, using theoretical analysis we introduce an analytical model describing how our device works, and show that model simulations produce the same RSS pattern as the experiment.

### 4.1 Design Challenge

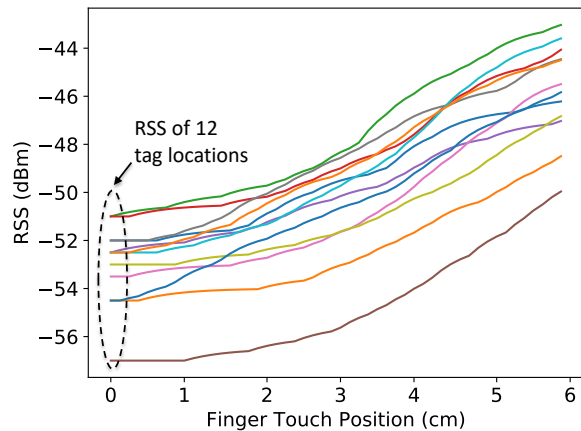
Earlier, we described previous systems using phase or RSS to detect finger touches on RFID tags [16, 17, 20]. To illustrate the limitations of these approaches, we perform a benchmark experiment using the setup shown in Fig. 5a, which is similar to RIO [20]. There are 12 test locations for an RFID tag (i.e., an Alien Squiggle RFID tag [5]) in a  $2.5 \times 2.5$  m<sup>2</sup> area, where the distance between two adjacent tag locations is  $\sim 0.6$  m. For each tag location, we measure RSS and



(a) Experiment setup to test reliability of using RSS or phase to detect finger touches on an RFID tag.



(b) RSS and phase of finger touches on an RFID tag when the tag is located across 12 different locations.



(c) The increase trend of RSS over 12 different tag locations when a finger swipes from position '0' to '6'.

**Figure 5: Comparing robustness of the absolute phase/RSS values and the increase/decrease trend of RSS values across different tag locations.**

phase when a finger touches 6 positions, which are separated by 1 cm, along a half antenna<sup>2</sup> of the tag.

The results are shown in Fig. 5b, where the  $x$ -axis shows 6 touch positions and a baseline case when there is no finger touch, and the  $y$ -axis shows the RSS or phase values. Each error bar shows the error 'whiskers' at 95% of the RSS or phase values measured at each finger touch position across 12 locations. Each box shows median and standard deviation of these measured values. As we can see, there are significant RSS and phase variations across tag

<sup>2</sup>Due to symmetry, the same phase/RSS pattern will occur on the other half antenna.

locations at any given finger touch position. This is because RSS and phase are a function of not only a finger touch, but also the tag location with respect to the reader [20, 24, 26].

The results show that the absolute phase can not be used to detect finger touches across different tag locations because all phase values of touching overlap the baseline phase of no-touch, as shown in Fig. 5(b). Similarly, the absolute RSS can not be used to reliably determine touch positions along tag because RSS values of adjacent touch positions overlap, as shown in Fig. 5(b). In fact, the absolute RSS can only be used to detect a single touch gesture robustly, and only on a certain area of the tag. For example, one could use a threshold of  $\sim 49$  dBm (i.e., the minimum baseline RSS value) to reliably detect a touch (one gesture) on the tag area between position 0 and position 2. Another option is to use finger sliding movements on the tag to enable a robust trinary touch detection given the ascending or descending pattern. Fig. 5c shows RSS values of a tag when a finger slide over its antenna. Each colour line shows the sliding RSS at one of the 12 tag locations. As we can see, all RSS values increase as the finger moves from position 0 to position 6, regardless of the tag location. Although this approach enable robust input detection even when tag location changes, but its inputs are very limited (1 or 2 finger gestures per tag). Unfortunately, because tags must be spaced half-wavelength apart (i.e., 16.4 cm for 915 MHz RFID signals) to avoid a coupling effect [22, 23], placing multiple tags on an input device is not an option. For example, one needs a 64 cm wide device to enable 10 inputs, using this approach.

To make a reasonably compact input device that can detect multiple finger inputs in a way that is robust to device location changes, we adapt the sliding finger gesture idea to an RFID transmission line structure introduced later.

## 4.2 Prototype Device Design

We introduce an RFID-based system capable of detecting finger gestures in a way that is robust to changes in device location or environment. Our key idea is that touching different positions along the transmission line changes the impedance matching between each chip and its antenna, changing the RSS for each chip. Therefore, by looking at relative RSS differences and the pattern of RSS changes, we can sense different sliding finger gestures while it is robust to location and environment change.

To validate this idea, we first constructed a prototype input device shown in Fig. 6. It has two RFID tags mounted on a thin cardboard substrate so they are spaced 16 cm apart. Each tag includes a commodity RFID chip [6] and a simple dipole antenna built by two 8.2 cm copper wires. To create a transmission line, the two RFID chips are connected together by two 1.6 mm wide copper strips. Note that we use different chips as the one used in the RFID tag tested in the last section. This is because the tag's chip is too small to solder a transmission line. Therefore, we use RFID chips with larger footprints. But we believe the RFID manufacturers can easily build our input device by using any RFID chips and adding a printable transmission line, just like they add a printable tag antenna to RFID chips.

Next, we conduct a benchmark experiment in a laboratory environment with one reader antenna mounted on the ceiling, and the device held by a user. The distance between the antenna and

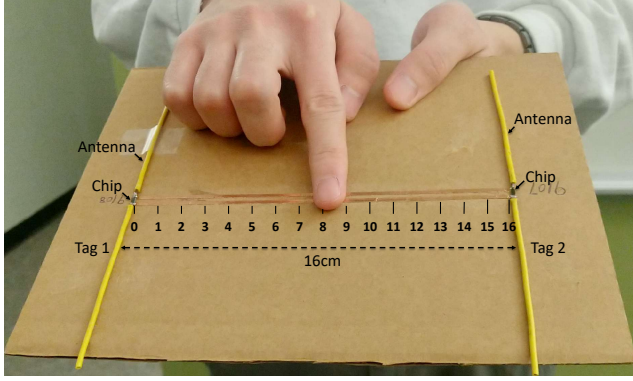


**Figure 6: Prototype device for sensing finger input: two RFID chips with dipole antennas are mounted 16 cm apart on a cardboard substrate, the chips are connected by copper tape to form a transmission line.**

the input device is 1.2 m. We label 17 touch positions along the transmission line on the device, spaced by 1 cm apart, as shown in Fig. 6. We then measure RSS values when a finger touches at each of these positions.

Fig. 7 shows the result of this experiment. The RSS values of each tag vary when a finger touches different positions. Interestingly, RSS values of each tag increase to a peak at a specific position (e.g., position 5 for tag 1) and then decreases after that.

Our hypothesis is that when placing a finger on the transmission line, the finger acts as a capacitor [13] and loads the transmission line. However, touching different positions of the transmission line creates different impedance to each RFID chip, resulting in changes of the matching efficiency in Eqn. (1). The added extra impedance is a function of the distance from the finger touch position to the chip. RSS reaches the maximum value when the added impedance helps the RFID chip to be matched to its antenna. To test this hypothesis, we theoretically analyze our design in the next section.

### 4.3 Theoretical Analysis And Model

We show through theoretical analysis why and how finger touches change the RSS of two tags on our input device. To do so, we consider a setup, where the following parameters are fixed or constants: the transmission power of the reader ( $P_t$ ), the distance between the reader and the input device ( $d$ ), the signal wavelength ( $\lambda$ ), the antenna gain  $G_t$ , and radar cross section  $\sigma$ . In this setup, Eqn. (1) can be simplified as:

$$RSS = 10 \log(1 - |\Gamma|) + C, \quad (5)$$

where,  $C$  is a constant and  $\Gamma$  is the reflection coefficient, related to the matching between the antenna and the loaded RFID chip. This equation implies that, for a given setup and hardware implementation, RSS is only a function of  $\Gamma$ . Thus, since our experiment shows that finger touches change the RSS, we hypothesis that finger touches change  $\Gamma$ , resulting in changes of RSS values.

To validate this hypothesis, we model the reflection coefficient  $\Gamma$  when a finger touches different positions of the input device. Fig. 8 shows an equivalent circuit of the device, where  $Z_a$ ,  $Z_c$  and  $Z_f$  are impedance of the tag's antenna, the chip and the finger. The  $l_1$  and  $l_2$  are distances of chip-1 and chip-2 from the finger position.

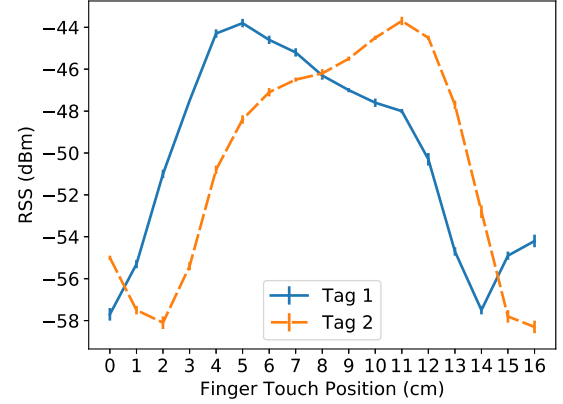


**Figure 7: RSS measured using the prototype device, by finger touch position along the transmission line.**

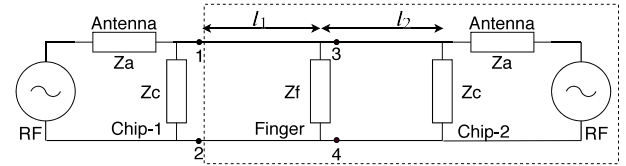


**Figure 8: An equivalent circuit of our input device.**

Therefore, the distance between two chips is  $L=l_1 + l_2$ . We only model the reflection coefficient  $\Gamma$  for tag 1. However, due to the symmetry of our device design, one can simply model  $\Gamma$  for tag 2.

We define  $Z_{12}$  as the impedance seen looking from left into port-12 (labeled as 1 and 2 in Fig. 8). Therefore, the chip's impedance  $Z_c$  is in parallel with  $Z_{12}$  (symbolized as  $Z_c || Z_{12}$ ) and then in series with the antenna's impedance  $Z_a$ . Followed by Eqn. (3), the reflection coefficient  $\Gamma$  of tag 1 can be expressed as:

$$\Gamma = \frac{Z_c || Z_{12} - Z_a}{Z_c || Z_{12} + Z_a} = \frac{\frac{Z_c Z_{12}}{Z_c + Z_{12}} - Z_a}{\frac{Z_c Z_{12}}{Z_c + Z_{12}} + Z_a}. \quad (6)$$

As we can see, the reflection coefficient  $\Gamma$  is only a function of  $Z_{12}$ , since  $Z_c$  and  $Z_a$  are constants.

Next, we analyze the relationship between  $Z_{12}$  and finger touch positions. Based on the transmission line theory explained in Section 3.2, the impedance  $Z_{12}$  can be expressed as:

$$Z_{12} = Z_0 \frac{Z_L + jZ_0 \tan(\beta l_1)}{Z_0 + jZ_L \tan(\beta l_1)}, \quad (7)$$

where,  $Z_0$  is the characteristic impedance, which is a constant for a given transmission line,  $\beta = \frac{2\pi}{\lambda}$ ,  $l_1$  is the distance of the finger from chip-1, and  $Z_L$  can be expressed as:

$$Z_L = \frac{Z_f Z_{34}}{Z_f + Z_{34}}, \quad (8)$$

where,  $Z_f$  is the impedance of the finger, and  $Z_{34}$  is the impedance seen looking into port-34 and can be expressed as:

$$Z_{34} = Z_0 \frac{Z'_L + jZ_0 \tan[\beta(L - l_1)]}{Z_0 + jZ'_L \tan[\beta(L - l_1)]}, \quad (9)$$

where  $L$  is the length of the transmission line and  $Z'_L$  can be expressed as:

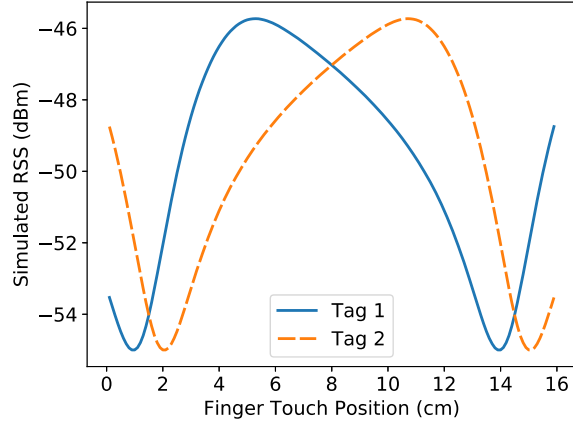


**Figure 9: RSS simulated by our model of the device, by finger touch position along the transmission line.**

$$Z'_L = \frac{Z_c Z_a}{Z_c + Z_a}. \quad (10)$$

By combining Eqn.(6)–(10), one can show that  $\Gamma$  is only function of the finger touch position, i.e.,  $\Gamma = f(l_1)$ . Further, using Eqn. (5), we can show that RSS is a function of the finger touch position, i.e.,  $RSS = g(l_1)$ , which validates our hypothesis.

**4.3.1 Model Simulation.** We run a simulation based our analysis to see how RSS changes for different finger touch positions ( $l_1$ ). Fig. 9 shows the result of this simulation. The pattern of RSS values follow the same pattern as our device experiment measurements, shown in Fig. 7. This consistency between the simulation and the real-world behaviour validates our model analysis, and provides the reason why and how a transmission line can be used for finger touch input in this way.

**4.3.2 Transmission Line Length.** The model and theoretical analysis also explains why we use a 16 cm long transmission line for our device. In Eqn. (7) and Eqn. (10), the parameter  $l_1$  relating to the transmission line length  $L$  ( $l_1 \leq L$ ), form an argument to the periodic  $\tan(\cdot)$  function. This means  $Z_{12}$  and  $Z_{34}$  will be periodic, and so will the resulting RSS. A periodic RSS response over the length of a transmission line would prevent reliable detection.

To avoid this, we need to limit the length of the transmission line. Consider the  $\tan(\beta l_1)$  term in Eqn. (7). Since  $\beta = \frac{2\pi}{\lambda}$ , the argument to  $\tan(\cdot)$  can be written in terms of wavelength  $\lambda$ , so  $\frac{2\pi}{\lambda} l_1 \in (-\frac{\pi}{2}, \frac{\pi}{2})$  and therefore  $l_1 \in (-\frac{\lambda}{4}, \frac{\lambda}{4})$ . This means  $l_1$  should less than  $\frac{\lambda}{2}$ , half a wavelength, to avoid periodicity. For the 915 MHz RFID signal, therefore, the maximum length for  $l_1$  and the transmission line  $L$  is 16.4 cm.

## 5 FINGER INPUT DETECTION

This section describes a versatile finger input vocabulary composed of ten sliding gestures enabled by a heuristics-based detection algorithm designed to be robust to changes in device location.

### 5.1 Gesture Definition

To motivate the use of increasing and decreasing patterns in RSS when a finger slides along the transmission line, we log RSS data

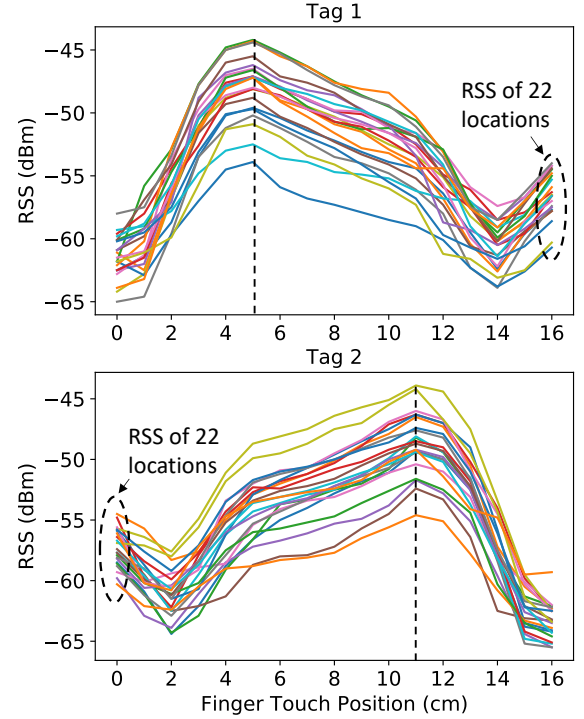


**Figure 10: RSS measurements of finger touches when our input device is located across 22 different locations.**

produced by our input device at different device locations. In a laboratory environment with a ceiling mounted antenna, a user holds the device and touches all 17 positions along the transmission line, one by one, as shown in Fig 6. At each position, the finger is held for 5 seconds. From the resulting 400 RSS samples per position, the average RSS is calculated as a data point. Importantly, this process is repeated at 22 different locations distributed across a  $2.5 \text{ m} \times 2.5 \text{ m}$  area, such that the distance between two adjacent locations is  $\sim 0.6 \text{ m}$ .

Fig. 10 shows the results for each tag separately for clarity. There are 22 colour lines, each shows the pattern of RSS for all 17 touch positions for one device location. We make two observations:

- *There is an increasing or decreasing pattern of RSS across finger positions that is independent of device location.* For example, when a finger moves from the 5 cm position to the 11 cm position, all RSS values of tag 1 decrease, and all RSS values of tag 2 increase.
- *The touch position where the RSS peaks is independent of device location.* In particular, the maximum RSS of tag 1 is always at the 5 cm touch position, and the maximum RSS of tag 2 is always at the 11 cm touch position.

**5.1.1 Ten Sliding Gestures.** Motivated by these observations, we define three sections along the transmission line, segmented by the 5 cm and 11 cm peak positions. For notational convenience, we label the boundary positions of the three sections as A, B, C, and D. Using these labels and sections, we define 10 different finger sliding gestures, where each is done by sliding a finger along a specific section of the transmission line. Fig. 11a illustrates the transmission line sections, boundary labels, and the sliding gestures as directional labelled arrows.

**Table 1: Signal features for the sliding finger gestures.**

Gesture	Peaks		Offset		Relative	Trend	
	$N_1$	$N_2$	$O_1$	$O_2$	$\Delta R$	$T_1$	$T_2$
AB	1	1	0	0	$> 0$	↗	↗
BA	1	1	0	0	$> 0$	↘	↘
BC	2	2	0	0	n/a	↘	↗
CB	2	2	0	0	n/a	↗	↘
CD	1	1	0	0	$< 0$	↘	↘
DC	1	1	0	0	$< 0$	↗	↗
ABC	1	1	1	0	n/a	↗↘	↗
CBA	1	1	1	0	n/a	↗↘	↘
BCD	1	1	0	1	n/a	↘	↗↘
DCB	1	1	0	1	n/a	↗	↗↘

For example, when a finger slides from A to B, we define it as the input gesture AB. Similarly, when a finger slides from A to B and continues to C, we define it as the input gesture ABC. When convenient, we also refer to pairs of gestures sharing section boundaries that are differentiated only by sliding direction with /, such as AB/BA for the related gestures A to B and B to A.

## 5.2 Gesture Signal Features

We introduce signal features which can be used to robustly detect the 10 gesture inputs, even if the device location changes. To do so, we first investigate how RSS of different gesture inputs look like. The top and bottom sub-figures of Fig. 11(b-k) show RSS and RSS derivative<sup>3</sup> of two tags for each gesture input, respectively. In each plot, the first 0.5 s shows the baseline RSS values, when there is no touch event. Then, a finger slides on the input device, changing the RSS values. Motivated by these measurements, we define four signal features (as shown in Table 1) which are robust to location changes of the input device and use them to recognize the 10 finger gesture inputs.

**Feature 1: Peaks ( $N_1, N_2$ ).** As we can see in Fig. 11, when a finger touches or releases the position B or C, the RSS changes very rapidly. This is because the RSS value when a finger touches the two positions is at its peak. These sudden changes create spikes in the derivatives of the RSS measurements, as shown in Fig. 11. Therefore, by counting the spikes in the derivatives of RSS, we can detect if the gesture has started or ended at position B or C. As we can see in Fig. 11, the derivatives of RSS for gestures AB/BA, CD/DC, ABC/CBA, and BCD/DCB have one spike, while the gestures BC/CB have two spikes. Hence, the first feature that we use in our detection algorithm is the number of peaks in the derivatives of RSS measurements. Table 1 summarizes the number of peak in derivatives of RSS values for different gestures, where  $N_1$  and  $N_2$  are the number of peaks for tag 1 and tag 2.

**Feature 2: Offset ( $O_1, O_2$ ).** As we can see in Fig. 13, for some gestures, such as AB/BA, BC/CB, and CD/DC, the maximum RSS and the spike of the RSS derivative occur at the same time. On the other hand, for some other gestures, such as ABC/CBA and BCD/DCB, there

<sup>3</sup>Let an RSS sequence be  $R = \{r_1, \dots, r_i, \dots, r_N\}$ , then the RSS derivative sequence is  $y_i = r_{i+1} - r_i, 1 < i < N - 1$ .

is an offset between when the maximum RSS is reached and the spike of the RSS derivative is registered. Using the input ABC as an example, the derivative of RSS of tag 1 spikes when a finger releases position C, while the maximum RSS happens when the finger is passing position B. We use this offset as the second feature. Since measuring the exact offset is challenging, we map them to a binary: 0 for ‘no offset’ and 1 for ‘offset’. In particular, if the offset is less than 20 samples (i.e., 100 ms), we consider it as ‘no offset’, otherwise, we consider it as ‘offset’. Table 1 summarizes the offsets for different gestures, where  $O_1$  and  $O_2$  represent the offset of tag 1 and tag 2, respectively.

**Feature 3: Relative RSS ( $\Delta R$ ).** The third feature is the relative RSS magnitude between two tags. This feature can particularly help in differentiating between AB/BA and CD/DC. This is because most RSS samples of tag 1 is larger than the RSS samples of tag 2 for gesture AB/BA, and most RSS samples of tag 1 is smaller than the RSS samples of tag 2 for gesture CD/DC, as shown in Fig. 11.

To compare the relative RSS relationship of two tags, we define an averaged RSS change  $\Delta R = \frac{1}{N} \sum_{i=1}^N (r_{1,i} - r_{2,i})$ , where  $r_{1,i}$  and  $r_{2,i}$  are RSS samples of tag 1 and tag 2, respectively. If  $\Delta R > 0$ , it implies that most RSS samples of tag 1 is larger than the RSS of tag 2; if  $\Delta R < 0$ , it implies that most RSS samples of tag 2 is larger than the RSS of tag 1. Table 1 summarizes values of  $\Delta R$  for inputs AB/BA and CD/DC.

**Feature 4: Trend ( $T_1, T_2$ ).** As shown in Fig. 11, during the time that a finger is sliding on the transmission line, RSS of each tag is either increasing or decreasing, depending on the gesture input. For example, for the input AB, RSS values of both tags increase. For the input BC, RSS values of tag 1 decreases while the RSS value of tag 2 increases. Therefore, we use the increase or decrease trend of RSS values as a feature for our gesture detection algorithm. Table 1 summarizes the RSS trend for all gesture inputs, where  $T_1$  and  $T_2$  represent the RSS trend (‘↗’ for increase and ‘↘’ for decrease) of tag 1 and tag 2, respectively.

## 5.3 Robustness in Multipath Environment

We have defined four features that are robust to changes in the device location and RF environment. In this section, we examine the impact of multipath effect on the robustness of the features.

In an indoor environment, RFID signals can travel from RFID tags to the reader’s antenna by two or more paths created by reflectors in the environment, such as walls and furniture. Since our device deploys two tags 16 cm apart, each tag may experience different multipath effects where RSS values vary for each tag differently when the device moves or environment changes. Although, this will not impact ‘Peak’, ‘Offset’, and ‘Trend’ features, it can change the relative RSS (i.e., Feature 3). Hence, in multipath environments ‘relative RSS’ feature can not help in differentiating gestures between AB/BA and CD/DC. To better understand the problem, Fig. 12a-b shows RSS values of two tags for the same gesture CD when performed at two different device locations with different amount of multipath signals, i.e., Location 1 with few multipath and Location 2 with rich multipath. As we can see, the RSS of tag 1 is higher than RSS of tag 2 at Location 1, which is true for the gesture CD. But their relative RSS relationship is opposite for Location 2, and

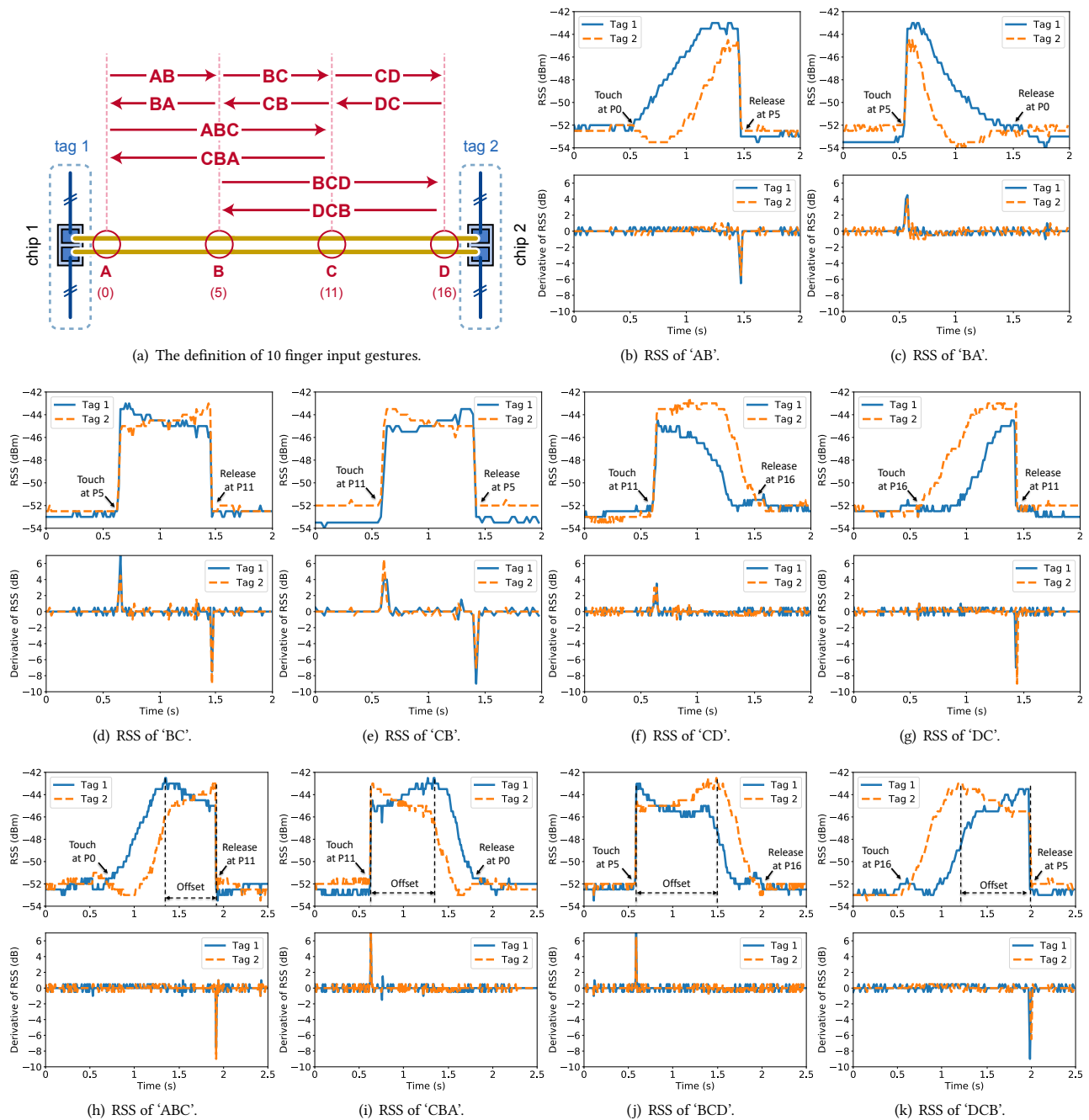


**Figure 11: Example sequences of RSS values and numerical derivatives resulting from the ten sliding finger gesture inputs.**

this opposite relative RSS matches with the gesture BA. The reason is that tags experience different multipath effects in different locations, resulting in different relative RSS values. This would introduce recognition errors when differentiating between gestures AB/BA and CD/DC in the multipath environment.

To solve this problem and enhance the robustness of ‘relative RSS’ (Feature 3) in multipath environments, we measure baseline RSS of each tag when there is no finger touch. Then we remove the baseline from all RSS measurements before computing the relative

RSS values. This process helps to remove the impact of multipath since multipath only adds a constant offset to RSS values. Fig. 12c shows the RSS change values of two tags after removing their baseline RSS for the same experiment as Fig. 12b. As we can see, once we remove the baseline RSS, the RSS of tag 1 becomes higher than tag 2, i.e., it matches with the ‘relative RSS’ feature in Fig. 12a. This suggests that removing the baseline RSS helps in making Feature 3 robust in multipath environment.

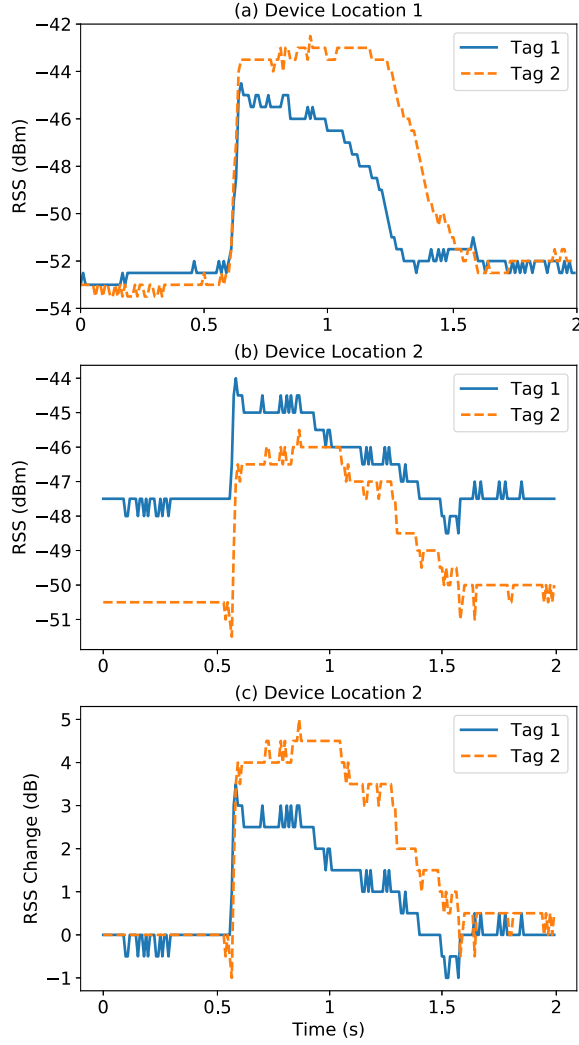


Figure 12: RSS and RSS change for gesture *cd* when the input device is located at different locations.

#### 5.4 Gesture Detection Algorithm

So far, we have introduced four signal features which are robust to location changes of the input device. Here, we introduce a decision tree classifier which can detect and classify gestures using the four features. The decision tree has four steps, as shown in Fig. 13:

- **Step 1:** In the first step, we use the feature ‘Peak’ to decide whether the performed gesture is *bc/cb* or other possible gestures. Recall that for gesture *bc/cb*, there are two peaks (i.e.,  $N_1 = 2, N_2 = 2$ ) in the derivatives of RSS, while for other gestures, there is only one peak (i.e.,  $N_1 = 1, N_2 = 1$ ).
- **Step 2:** Next, we use the feature ‘Offset’ to decide whether the gesture is one of  $\{AB/BA, CD/DC\}$  or one of  $\{ABC/CBA, BCD/DCB\}$ . As mentioned earlier, when a finger slides through position *b* or *c*, there may be a time offset between the maximum RSS and the spike in RSS derivatives. Specifically, if the gesture is one of  $\{ABC/CBA, BCD/DCB\}$ , one of offsets will be non-zero (i.e.,  $O_1 + O_2 = 1$ ). Otherwise, both offsets will be zero (i.e.,  $O_1 + O_2 = 0$ ).

- **Step 3:** This step has two sub-steps. First, we decide whether the gesture is *AB/BA* or *CD/DC*. To do so, we use the feature ‘Relative RSS’. As already explained in Table 1, this feature is positive (i.e.,  $\Delta R > 0$ ) when the gesture is *AB/BA* and it is negative (i.e.,  $\Delta R < 0$ ) when the gesture is *CD/DC*. Second, we differentiate between *ABC/CBA* and *BCD/DCB*. To do so, we use the feature ‘Offset’. As shown in Table 1, for gesture *ABC/CBA*,  $O_1 = 1$  and  $O_2 = 0$ , while for gesture *BCD/DCB*,  $O_1 = 0$  and  $O_2 = 1$ .
- **Step 4:** Finally, we distinguish the direction of two gestures that share section boundaries using the ‘Trend’ feature. Consider *AB/BA* as an example. The trend for tag 1 is upward (i.e.,  $T_1 = \nearrow$ ) for the gesture *AB*, while it is downward for the gesture *BA* (i.e.,  $T_2 = \searrow$ ). As shown in Fig. 13, similar decisions can be made for other pairs of related gestures.

## 6 IMPLEMENTATION

The design and fabrication of our finger input device was explained in Section 4, here we describe other system details.

We use an Impinj Speedway R420 RFID reader [10] without any hardware or firmware modification. The RFID reader has four antenna ports and operates in a frequency range of 902.75–927.25 MHz. The default antennas used by the reader are directional, with 9 dBi gain and  $70^\circ$  elevation and azimuth beam widths [1]. The reader and RFID chips/tags are compatible with EPC Gen2 standard protocol [11]. The multiple reader antennas work in a time-division multiplexing mode. The time slot for each antenna is  $\sim 200 \mu s$  [10].

All data logging and detection algorithms are implemented in C# and Python code running on a laptop (Intel i5-6200U 2.4GHz CPU, 8GB RAM). The laptop is connected to the RFID reader through an Ethernet cable for communication. Backscatter packets for all tags received by the reader are forwarded to the laptop for processing. The size of an RFID backscatter packet is small since it only contains the tag’s ID (12 bytes at most) [10].

## 7 EVALUATION

In this section, we evaluate the performance of our system when differentiating between the 10 input gestures under different conditions. We first report on a main experiment examining recognition performance across different device locations in two different room environments. After, we discuss focused follow-up experiments examining the impact of other factors: reader antenna distance, finger sliding speed, and changes in the RF environment caused by nearby moving people.

The demo video is available on YouTube [28]. The source code and sample data of our input gesture detection algorithm are available on GitHub [27].

### 7.1 Experiment 1: Device Location Changes

The performance of gesture detection when the location of the device changes is a primary validation of our approach and system.

**7.1.1 Method.** The experiment is conducted in two environments, a smaller space in a laboratory and a mid-sized classroom (see Fig. 14). In the laboratory setup, one antenna is mounted on the ceiling creating a coverage area of  $2.5 \times 2.5 \text{ m}^2$ . In the classroom, four antennas are mounted under ceiling lights to cover  $5 \times 5 \text{ m}^2$ , equivalent to 4 rows of tables, or 24 seats.

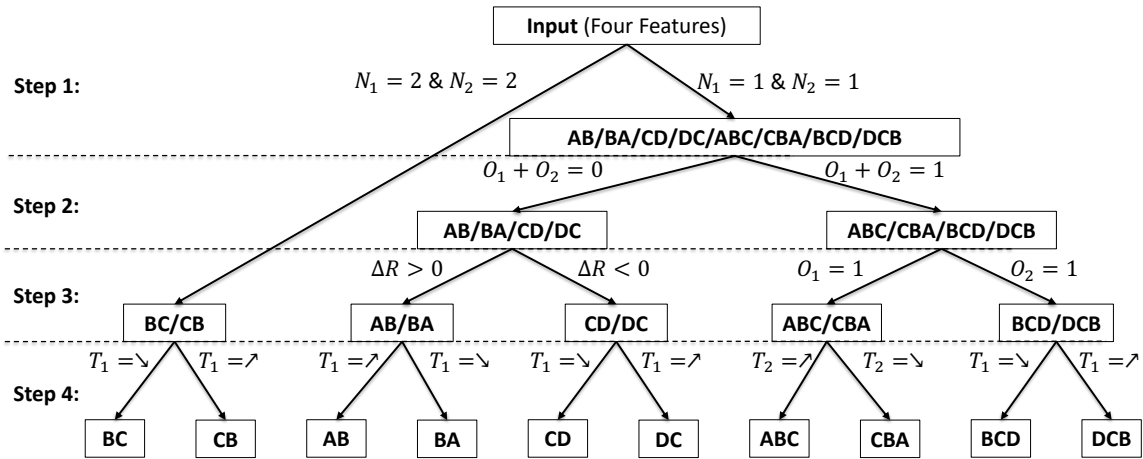


Figure 13: Sliding finger gesture detection algorithm decision tree.

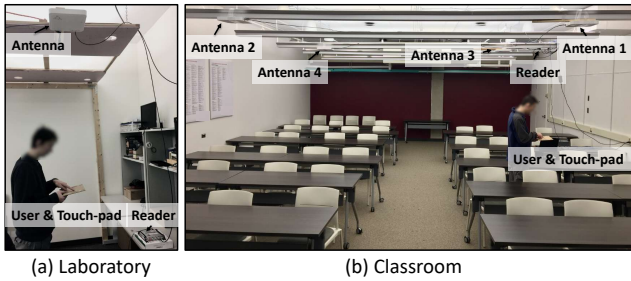


Figure 14: Experiment settings: (a) one antenna in a laboratory area; (b) Four antennas in a classroom.

The protocol requires the user to perform all 10 input gestures, each one 10 times, with the device held at 12 locations in the laboratory and 36 locations in the classroom. Each location is chosen pseudo-randomly such that it is within the coverage area and the distance between adjacent test locations is approximately 0.5 m. At any location, the distance from the device to the nearest reader antenna is between 0.7 and 1.6 m.

In summary, for the laboratory there are 12 locations  $\times$  10 inputs  $\times$  10 trials = 1,200 test samples, and for the classroom, there are 36 locations  $\times$  10 inputs  $\times$  10 trials = 3,600 test samples.

**7.1.2 Results.** We use a *Confusion Matrix* [8] to examine individual accuracy for detecting each gesture input and *Precision* and *recall* [8] for overall performance. A high recall means there are many true positives with few false negatives, and high precision means there are many true positives with few false positives.

Fig. 15 shows the recognition accuracy for each input gesture across all device locations in each of the two environments. In both environments, the system achieves at least 91% identification accuracy, and in many cases much higher. For example, in the classroom, 7 out of 10 gestures have an accuracy of 95% or more. Overall performance is very good. Detection in the laboratory has 95.2% precision and 94.5% recall, and detection in the classroom has 95.4% precision and recall 94.6%.

Detected Gesture	Input Gesture									
	AB	BA	BC	CB	CD	DC	ABC	CBA	BCD	DCB
AB	0.92	0	0	0	0	0	0	0	0	0.01
BA	0	0.98	0.05	0	0	0	0	0	0	0.03
BC	0	0	0.92	0	0	0	0.01	0	0	0.02
CB	0	0	0	0.93	0	0.02	0	0	0	0.05
CD	0	0.02	0	0	1	0.02	0	0	0.02	0
DC	0.03	0	0	0	0	0.93	0.02	0	0	0.02
ABC	0	0	0.03	0	0	0	0.97	0.02	0	0
CBA	0	0	0	0	0	0.03	0	0.95	0	0
BCD	0	0	0	0	0	0	0	0.03	0.93	0
DCB	0.05	0	0	0.07	0	0	0	0	0	0.92

(a) Laboratory setting with 12 device locations.

Detected Gesture	Input Gesture									
	AB	BA	BC	CB	CD	DC	ABC	CBA	BCD	DCB
AB	0.96	0	0	0	0	0.01	0	0	0	0.02
BA	0	0.97	0	0	0	0	0	0	0	0
BC	0.02	0	0.96	0	0.04	0	0.05	0	0.03	0
CB	0.01	0.01	0	0.91	0	0.01	0	0.02	0	0.06
CD	0	0	0	0	0.95	0	0	0	0	0
DC	0	0	0	0	0	0.98	0.02	0	0	0.01
ABC	0	0	0.01	0	0	0	0.93	0	0	0
CBA	0	0.02	0	0.05	0	0	0	0.98	0	0
BCD	0	0	0.03	0.01	0.01	0	0	0	0.97	0
DCB	0.01	0	0	0.03	0	0	0	0	0	0.91

(b) Classroom setting with 36 device locations.

Figure 15: Confusion matrices showing the input gesture detection accuracy across multiple locations.

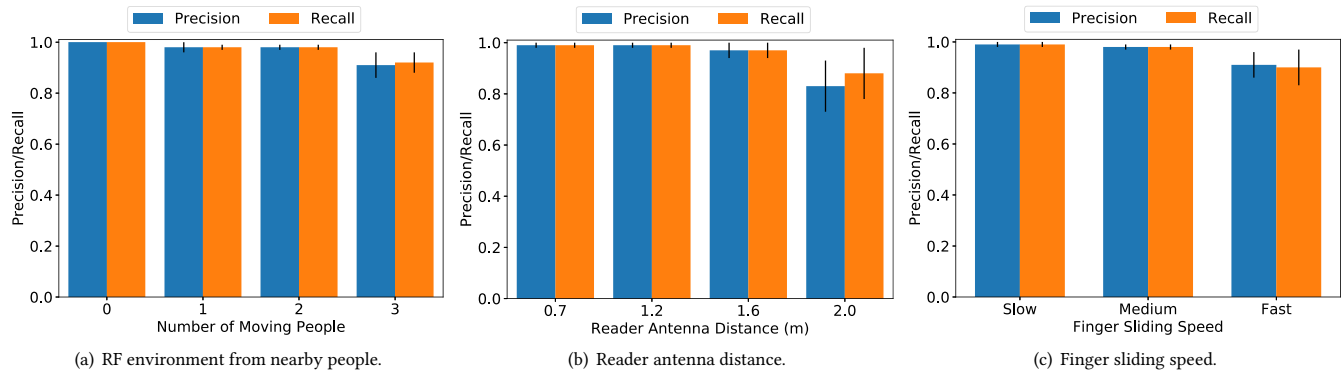


Figure 16: Results for Experiments 2, 3, and 4.

## 7.2 Experiment 2: RF Environment Variations

Variations in the RF environment can also affect RSS, which could introduce detection errors. We test a common cause of RF environment changes, when people move nearby the experimental setup.

**7.2.1 Method.** Using the laboratory environment, we fix the location of the user operating the input device beneath the antenna, and ask other people to move nearby with a normal walking speed. We do this with 0, 1, 2, and 3 people, forming a ‘people’ experimental factor. The distance between the moving people and the input device is controlled to be within 0.2 m to 1.0 m, and the people continue to move as the user interacts with the input device. For each number of people, the user performs 10 trials of the 10 input gestures. Note, although the line of sight path does not get blocked with people since the reader antenna is mounted on the ceiling, signals are still affected by changes in the RF environment resulting from people moving near by. In summary, 4 levels of ‘people’  $\times$  10 gestures  $\times$  10 trials = 400 test samples.

**7.2.2 Results.** Fig. 16a shows the precision and recall of detecting all gesture inputs for each number of people moving nearby. Both precision and recall are higher than 90%, even with three moving people. This suggests that this source of RF environment variation does not have a great impact on the reliability of our system.

## 7.3 Experiment 3: Reader Antenna Distance

A user will hold the device at different heights and locations, resulting in changes in the distance from the input device to the reader antenna. In this experiment, we evaluate this impact on input detection accuracy.

**7.3.1 Method.** Using the laboratory environment with a ceiling mounted antenna, the user with the device stands at the projection location of the reader antenna on the ground. We introduce a ‘distance’ factor where the user holds the device such that it is either 0.7 m, 1.2 m, 1.6 m, or 2 m away from the reader antenna. At each distance, all 10 gestures are performed one by one, with each gesture performed 10 times. In summary, for this experiment, there are 4 levels of ‘distance’  $\times$  10 gestures  $\times$  10 trials = 500 test samples.

**7.3.2 Results.** Fig. 16b shows the results. When the distance is less than 2 m, both precision and recall are higher than 97%. At 2 m, precision and recall drop to 81% and 85%. This reduction in accuracy

is due to noisy RSS readings caused by the lower signal-to-noise ratio (SNR) at this range. Note the working range of the comparable RIO finger input system is less than 2 m with unmodified commodity tags, and less than 1.5 m with customized tags [20]. In general, the working range may be increased by using a higher quality RFID chip that is more sensitive, designing a better tag antenna with greater impedance matching, or optimizing reader transmission power over multiple antennas [19, 31].

## 7.4 Experiment 4: Finger Sliding Speed

Different users may slide their fingers at different speeds along the transmission line. In this experiment, we evaluate how sliding speeds affects detection accuracy.

**7.4.1 Method.** Using the laboratory environment, with the user standing at a fixed location under a ceiling mounted antenna, we test three finger sliding speeds: ‘Fast’ which covers the 5 cm distance of one segment gestures (e.g. AB) in less than 1 second; ‘Slow’ which covers a 5 cm distance in more than 2 seconds; and ‘Medium’ in which the sliding speed is between the fast and the slow. For each sliding speed, the user performs 10 trials of all 10 gestures, resulting in 300 test samples.

**7.4.2 Results.** Fig. 16c shows the results. Both precision and recall are higher than 90% for all three sliding speeds, but the accuracy decreases when the sliding speed is very fast. We believe this is primarily a factor of reader reading rate, which could be increased. The reading rate of our reader is  $\sim$ 60 samples per tag per second. However, the reading rate can be simply improved by using a faster reader. For example, the reading rate of the LRU1002 reader is 241 samples per tag per second [12]. This reading rate enables our system to reliably detect even fast gestures which are performed in 0.25 second or slower.

Finally, note that we assume the user does not significantly move during sliding a finger on the input device. Although, slow movement is fine, if the user moves quickly, while they are performing a gesture, the RSS pattern will change because of both movement and the gesture, and hence our system can not robustly detect the gesture. However, since the time of each gesture is short, this problem does not happen very often in practice. Furthermore, one can also simply address this problem by designing an RFID reader which has much higher reading rate.

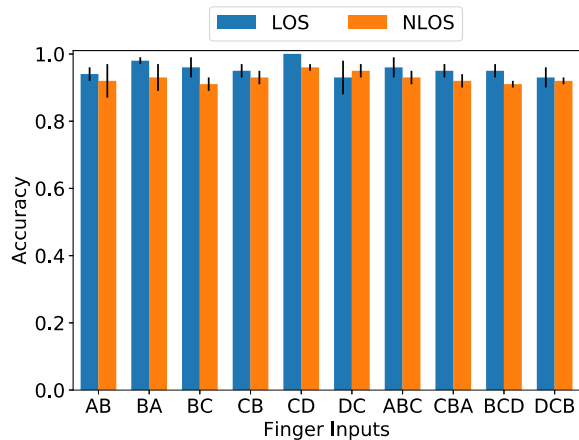


Figure 17: Results of Experiment 5: performance comparisons in LOS and NLOS.

## 7.5 Experiment 5: Non-Line-of-Sight Setting

The evaluation settings above assume line-of-sight (LOS) from RFID tags to the reader antenna with few multipaths. When reader antennas are placed in the ceiling, this assumption is reasonable for many use cases. However, in this experiment we evaluate a more extreme non-line-of-sight (NLOS) setting, when a large object blocks the direct path between the device and the reader antenna.

**7.5.1 Method.** The blocking object is a large box (1.2 m  $\times$  1.0 m  $\times$  0.3 m) covered in aluminum foil, which is placed in a 1.4 m space between the user with the device and the reader antenna. In this NLOS setting, the user performs all ten gestures one by one, repeating each one 10 times. For comparison, this is repeated for a LOS setting by removing the blocking box. In summary, 2 settings (NLOS and LOS)  $\times$  10 gestures  $\times$  10 trials = 200 test samples.

**7.5.2 Results.** Fig. 17 shows that input detection accuracy decreases slightly in the NLOS setting, but the detection accuracy remains higher than 90% for all gestures. This suggests our approach is robust even in the NLOS scenario. This is because our input gesture detection algorithm uses the relative trend of RSS values, while NLOS settings mostly impact absolute RSS values.

## 8 LIMITATIONS AND FUTURE WORK

There are limitations to our system and approach that suggest further investigation and possible extensions:

**Detecting more input gestures.** Our current prototype device detects only 10 different input gestures using two RFID chips. However, the system may be extended to detect more inputs using the same basic technique in different configurations with multiple chips. For example, one can place three RFID chips on vertices of a triangle, and connect them using three transmission lines. This could detect 10 input gestures per edge, enabling an input device capable of detecting 30 gestures. Another possible configuration is a 2D grid of transmission lines. We are currently exploring this approach, noting it likely requires a new algorithm design applicable to a new and greatly expanded gesture set.

**Supporting multiple input devices.** Our device uses two commodity RFID chips. A typical RFID reader can read up to 240 tags

per second [12]. Thus, we can support up to 120 input devices simultaneously. This can be improved further by using faster readers.

**System Cost.** Our input device uses a transmission line and two RFID chips which cost less than a dollar. For the RFID reader, we use an Impinj R420 reader which costs  $\sim$ 1500 USD. It is an industrial RFID reader which can support up to 32 antennas, and provides both RSS and phase measurements. However, since our system requires only RSS readings and a single antenna, one can use a less expensive reader. For example, the SR681 RFID reader is 199 USD, and has a range up to 8 m [33]. Designing low-cost, compact RFID reader tailored to a smart device IoT setting using specialized devices like our system is an interesting future research direction.

**Robustness to different users.** Although, our current design is evaluated with one user, we believe it works also for different users since it relies on the pattern of RSS changes instead of absolute RSS. In particular, different users (with different height, sliding speed, BMI, finger thickness) cause variations in the absolute RSS values which will automatically be removed since our algorithm uses the pattern of RSS changes. For example, in Section 7.3, we show our system achieves high accuracy for different user heights when the tag-reader distance is less than 2m. Furthermore, in Section 7.4 we show our system is robust to different finger sliding speeds.

**Impact of different substrate materials.** Our prototype uses cardboard as the device substrate, but other non-metal materials such as plastics, wood, and glass can also work in our design. Any non-metal material should not significantly alter the electromagnetic field and RSS readings of RFID tags. Past work has empirically shown that many insulator surface materials, such as a book or wood, did not change the absolute RSS of unmodified RFID tags [24]. However, a metallic material or coating is likely problematic, since it causes a large signal attenuation, reducing the operating range of an RFID tag significantly.

## 9 CONCLUSION

This paper presents an RFID-based system to detect a diverse range of sliding finger input gestures, while remaining robust to device location changes and typical RF environment changes caused by nearby people. The key idea we propose, analyze, and implement is creating a transmission line as a touch sensor between two RFID tags, and using the characteristics of RSS values over time for heuristics-based recognition. The method and system presented in this paper can easily be adopted by designers and researchers to create simple, low-cost, and battery-free input solutions for a wide range of smart devices and other real world applications.

## 10 ACKNOWLEDGMENTS

We thank the shepherd and anonymous reviewers for their valuable feedback on this paper. We thank “NRC-University of Waterloo Collaboration Center (NUCC) program 927517” and “NSERC” for their support.

## REFERENCES

- [1] atlasRFIDstore. 2018. RFMAX RFID Antenna. <https://www.atlasrfidstore.com/rfmax-rfid-race-timing-antenna-kit-15-ft-cable/>. Last accessed: July 27, 2019.
- [2] Rachel Bainbridge and Joseph A Paradiso. 2011. Wireless hand gesture capture through wearable passive tag sensing. In *Proc. IEEE International Conference on Body Sensor Networks*. 200–204.

- [3] Constantine A Balanis. 2011. *Modern antenna handbook*. John Wiley & Sons.
- [4] Christophe Caloz and Tatsuo Itoh. 2005. *Electromagnetic metamaterials: transmission line theory and microwave applications*. John Wiley & Sons.
- [5] Alien Technology Corp. 2017. UHF ALN-9740 tag. <https://www.atlasrfidstore.com/alien-squiggle-rfid-white-wet-inlay-aln-9740-higgs-4/>. Last accessed: July 17, 2018.
- [6] Murata Electronics. 2020. RFID LXMS31ACNA. <https://www.digikey.ca/product-detail/en/LXMS31ACNA-011/490-11802-1-ND/5333642/?itemSeq=313684124>. Last accessed: January 17, 2020.
- [7] Chuhan Gao, Yilong Li, and Xinyu Zhang. 2018. LiveTag: Sensing Human-Object Interaction through Passive Chipless WiFi Tags. In *Proc. USENIX NSDI*. 60–63.
- [8] geeksforgeeks. 2018. Confusion Matrix in Machine Learning. <https://www.geeksforgeeks.org/confusion-matrix-machine-learning/>. Last accessed: January 27, 2020.
- [9] Impinj. 2005. Low Level User Data Support. <https://support.impinj.com/hc/en-us/articles/202755318-Application-Note-Low-Level-User-Data-Support>. Last accessed: February 24, 2020.
- [10] Impinj. 2010. Impinj R420 Readers. <http://www.Impinj.com/products/readers/>. Last accessed: June 27, 2018.
- [11] EPCglobal Inc. 2007. Low Level Reader Protocol, Version 1.0. 1. (2007).
- [12] FEIG ELECTRONICS Inc. 2017. LRU1002 Fixed UHF Long-Range Reader. <https://rfdreadernews.com/wp-content/uploads/2017/04/FEIG-Whitepaper-Benchmark-Testing-of-UHF-RFID-Readers.pdf>. Last accessed: July 17, 2019.
- [13] Niels Jonassen. 1998. Human body capacitance: static or dynamic concept. In *Proc. of Electrical Overstress Electrostatic Discharge Symposium*. 111–117.
- [14] Keiko Katsuragawa, Ju Wang, Ziyang Shan, Ningshan Ouyang, Omid Abari, and Daniel Vogel. 2019. Tip-Tap: Battery-free Discrete 2D Fingertip Input. In *Proc. ACM UIST*. 1045–1057.
- [15] David Kim, Otmar Hilliges, Shahram Izadi, Alex D Butler, Jiawen Chen, Iason Oikonomidis, and Patrick Olivier. 2012. Digits: freehand 3D interactions anywhere using a wrist-worn gloveless sensor. In *Proc. ACM UIST*. 167–176.
- [16] Hanchuan Li, Eric Brockmeyer, Elizabeth J Carter, Josh Fromm, Scott E Hudson, Shwetak N Patel, and Alanson Sample. 2016. PaperID: A technique for drawing functional battery-free wireless interfaces on paper. In *Proc. ACM CHI*. 5885–5896.
- [17] Hanchuan Li, Can Ye, and Alanson P Sample. 2015. IDSense: A human object interaction detection system based on passive UHF RFID. In *Proc. ACM CHI*. 2555–2564.
- [18] Jaime Lien, Nicholas Gillian, M Emre Karagozler, Patrick Amihoud, Carsten Schwesig, Erik Olson, Hakim Raja, and Ivan Poupyrev. 2016. Soli: Ubiquitous gesture sensing with millimeter wave radar. *ACM Transactions on Graphics (TOG)* 35, 4 (2016), 142.
- [19] Yunfei Ma, Zhihong Luo, Christoph Steiger, Giovanni Traverso, and Fadel Adib. 2018. Enabling deep-tissue networking for miniature medical devices. In *Proc. ACM SIGCOMM*. 417–431.
- [20] Swadhin Pradhan, Eugene Chai, Karthikeyan Sundaresan, Lili Qiu, Mohammad A Khojastepour, and Sampath Rangarajan. 2017. RIO: A Pervasive RFID-based Touch Gesture Interface. In *Proc. ACM MobiCom*. 261–274.
- [21] Ultraleap. 2020. Leap Motion. <https://www.leapmotion.com>. Last accessed: January 17, 2020.
- [22] Jon W Wallace and Michael A Jensen. 2004. Mutual coupling in MIMO wireless systems: A rigorous network theory analysis. *IEEE transactions on wireless communications* 3, 4 (2004), 1317–1325.
- [23] Ge Wang, Haofan Cai, Chen Qian, Jinsong Han, Xin Li, Han Ding, and Jizhong Zhao. 2018. Towards replay-resilient RFID authentication. In *Proc. ACM Mobicom*. 385–399.
- [24] Ju Wang, Liqiong Chang, Omid Abari, and Srinivasan Keshav. 2019. Are RFID Sensing Systems Ready for the Real World?. In *Proc. ACM Mobisys*. 366–377.
- [25] Ju Wang, Liqiong Chang, Shourya Aggarwal, Omid Abari, and Srinivasan Keshav. 2020. Soil moisture sensing with commodity RFID systems. In *ACM Proceedings of the 18th International Conference on Mobile Systems, Applications, and Services (MobiSys)*. 273–285.
- [26] Jue Wang and Dina Katabi. 2013. Dude, where’s my card?: RFID positioning that works with multipath and non-line of sight. In *ACM SIGCOMM*. 51–62.
- [27] Ju Wang, Jianyan Li, Mohammad Hossein Mazaheri, Keiko Katsuragawa, Daniel Vogel, and Omid Abari. 2020. Code and Data of Sensing Finger Input Using RFID. <https://github.com/RFIDInput/Sensing-Finger-Input-Using-An-RFID-Transmission-Line>. Last accessed: June 27, 2020.
- [28] Ju Wang, Jianyan Li, Mohammad Hossein Mazaheri, Keiko Katsuragawa, Daniel Vogel, and Omid Abari. 2020. Demo Video of Sensing Finger Input Using RFID. [https://youtu.be/L\\_5GfVamZMs](https://youtu.be/L_5GfVamZMs). Last accessed: June 27, 2020.
- [29] Jue Wang, Deepak Vasisht, and Dina Katabi. 2014. RF-IDraw: virtual touch screen in the air using RF signals. In *Proc. ACM Sigcomm*. 235–246.
- [30] Ju Wang, Jie Xiong, Hongbo Jiang, Xiaojiang Chen, and Dingyi Fang. 2017. D-Watch: Embracing “Bad” multipaths for device-free localization with COTS RFID devices. *IEEE/ACM Transactions on Networking (TON)* 25, 6 (2017), 3559–3572.
- [31] Jingxian Wang, Junbo Zhang, Rajarshi Saha, Haojian Jin, and Swarnun Kumar. 2019. Pushing the range limits of commercial passive rfids. In *Proc. of USENIX NSDI*. 301–316.
- [32] Wikipedia. 2019. Reflection coefficient. [https://en.wikipedia.org/wiki/Reflection\\_coefficient](https://en.wikipedia.org/wiki/Reflection_coefficient). Last accessed: January 27, 2020.
- [33] Yanzeo. 2020. Yanzeo SR681 UHF RFID Reader. [https://www.amazon.com/Yanzeo-SR681-Outdoor-Antenna-Integrated/dp/B072N4P2MG/ref=sr\\_1\\_3?crd=271112C7X9B4&dchild=1&keywords=uhf+reader&qid=1593475974&sprefix=uhf+rea%2C148&sr=8-3](https://www.amazon.com/Yanzeo-SR681-Outdoor-Antenna-Integrated/dp/B072N4P2MG/ref=sr_1_3?crd=271112C7X9B4&dchild=1&keywords=uhf+reader&qid=1593475974&sprefix=uhf+rea%2C148&sr=8-3). Last accessed: June 27, 2020.